ACS Catalysis

Research Article

pubs.acs.org/acscatalysis

How Nitrogen-Doped Graphene Quantum Dots Catalyze Electroreduction of CO_2 to Hydrocarbons and Oxygenates

Xiaolong Zou,*[,†] Mingjie Liu,[‡] Jingjie Wu,[‡] Pulickel M. Ajayan,[‡] Jia Li,[§] Bilu Liu,[†] and Boris I. Yakobson*[,‡]

[†]Low-dimensional Materials and Devices Laboratory, Tsinghua-Berkeley Shenzhen Institute, Tsinghua University, Shenzhen, Guangdong 518055, People's Republic of China

[‡]Department of Materials Science and NanoEngineering, Rice University, Houston, Texas 77005, United States

[§]Institute of Advanced Materials, Graduate School at Shenzhen, Tsinghua University, Shenzhen, Guangdong 518055, People's Republic of China

ABSTRACT: Recently, metal-free nitrogen-doped graphene quantum dots (NGQDs) have been experimentally demonstrated to electrochemically convert CO_2 into high-order hydrocarbons and oxygenates, after more than 30 years since the identification of copper as an active metal catalyst for such conversions. However, the physicochemical principle of such catalytic activity for NGQDs has remained unclear. Here, by performing first-principles simulations, we have systematically investigated the underlying mechanisms governing the whole process. The introduction of N atoms into edges of graphene quantum dots enhances their bonding with *COOH, effectively promoting the reduction of CO_2 to CO. By including the influences of water, we reveal that the selective production of CH_4 over CH_3OH is attributed to a much lower kinetic barrier for the conversion of adsorbed *CH_2OH to *CH_2 via water molecule mediated proton shuttling. Further, adsorbed *CH_2 provides active sites for the coupling with CO to generate C_2 products, including both C_2H_4 and C_2H_5OH. These results offer theoretical insights into the reduction pathways of CO_2 on NGQDs, which may facilitate the design of metal-free carbon-based catalysts for efficient CO_2 reduction.

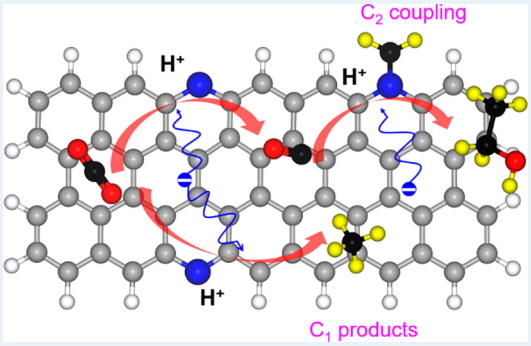

KEYWORDS: *CO_2 reduction reaction, graphene quantum dot, nitrogen doping, reaction kinetics, first-principles simulations*

1. INTRODUCTION

The electrochemical reduction of CO_2 to value-added chemicals and fuels has gained considerable research interest recently, largely due to ever-increasing CO_2 emissions from combustion of fossil fuels causing significant damage to our environment. Among the various catalytic metals investigated for the CO_2 reduction reaction (CRR) in an electrochemical setting, Cu is the only candidate which is capable of reducing CO_2 to hydrocarbons and oxygenates, such as CH_4, C_2H_4, and C_2H_5OH, although in a wide distribution and low yield for each product.[1−3] In order to further advance practical applications, great efforts have been devoted to the understanding of underlying mechanisms both experimentally and theoretically, in particular the product distribution and structure−activity relationship.[4−24] Koper et al. have formulated the current trends of understanding the CRR processes on Cu[25] and concluded that the suboptimal adsorption energies of intermediate states on Cu lead to low efficiency and selectivity, limiting its scalable applications. To overcome the high overpotential and poor selectivity of Cu, it is urgent to extensively search more efficient substitutes including metal-free catalysts.[26,27]

Rapid development in synthesis methods for various carbon nanomaterials has rendered them the most popular metal-free catalysts for different reactions. For example, nonmetal heteroatom-doped carbon materials have shown great efficiency in reducing oxygen molecules.[28−32] In particular, nitrogen doping[30−33] could break up the charge neutrality of carbon materials through introduction of abundant electrons, which significantly enhances the reduction activities of carbon-based catalysts. Inspired by these experiments, researchers have recently investigated the CRR on different nitrogen-doped carbon nanomaterials, including carbon fibers,[34] carbon nanotubes (CNTs),[35,36] and graphene foam.[37] It has been demonstrated that these carbon-based catalysts can effectively reduce CO_2. Taking advantage of quantum and edge effects, other forms of carbon nanomaterials ranging from carbon nanoribbons (CNRs)[38] to carbon quantum dots (CQDs)[39,40] could be adopted to further improve catalytic performance. For example, boron- and nitrogen-codoped graphene nanoribbons have been shown to significantly enhance the activities of the

Received: June 6, 2017
Revised: July 26, 2017
Published: August 8, 2017

DOI: 10.1021/acscatal.7b01839
ACS Catal. 2017, 7, 6245−6250

oxygen reduction reaction,[41] due to favorable modifications of both atomic and electronic structures of carbon nanostructures near the edges.

Here, we carry out extensive first-principles simulations to investigate CRR processes on N-doped graphene quantum dots (NGQDs). We show that NGQDs can electrochemically convert CO_2 to various hydrocarbons and oxygenates, including CH_4, C_2H_4, and C_2H_5OH, which makes NGQDs a valuable alternative to Cu for CO_2 reduction. These conversions begin with effective reduction of CO_2 to CO, promoted by enhanced binding between *COOH and NGQDs. By considering both the thermodynamic and kinetic properties of intermediate products, we have unraveled the underlying mechanisms of the selective production of CH_4 over CH_3OH. It is found that water-assisted H shuttling significantly reduces the barrier for the generation of $*CH_2$, the precursor for CH_4. Moreover, we propose a possible pathway for the formation of C_2 products, critically depending on the coupling of C_1 products—$*CH_2$ and CO. Further experimental verifications of these mechanisms could greatly facilitate the optimization of carbon-based catalysts for the CRR.

2. DENSITY FUNCTIONAL THEORY SIMULATIONS

Employing the Vienna ab initio Simulation Package (VASP),[42,43] all calculations were performed using Perdew–Burke–Ernzerhof (PBE) parametrization[44] of generalized gradient approximation to density functional theory (DFT) with projector-augmented wave potentials.[45,46] Different nitrogen (N)-doped carbon nanomaterials, including GQDs, graphene, and (5, 5) CNTs, were considered to investigate the distinct properties of GQDs brought about by edge effects. Our previous studies have shown that pyridinic N plays a key role in enhancing the catalytic performance of carbon materials,[35,37] and the high catalytic activities of edge pyridinic N in the oxygen reduction reaction have been clearly confirmed through controlled doping.[47] In addition, as the synthesized NGQDs have predominant pyridinic N,[48] we therefore focus on pyridinic N doping in the present study. Figure 1 shows our

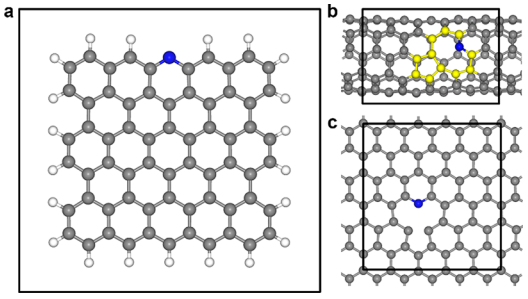

Figure 1. Structural models and unit cells for (a) NGQDs, (b) N-doped CNTs, and (c) N-doped graphene. Gray, blue, and white spheres represent carbon, nitrogen, and hydrogen atoms, respectively. The single vacancy in CNT is highlighted in yellow. The black rectangles schematically show the unit cells for simulations.

structural models for these systems, and the pyridinic N is introduced to the edge sites of GQDs or single-vacancy sites in CNTs and graphene. The unit cell sizes for NGQDs, CNTs, and graphene are 25 × 25 × 15, 20 × 20 × 12.35, and 12.16 × 12.92 × 15 Å, respectively. These choices ensure the distance between the largest adsorbate and its images is greater than 9.5 Å, which keeps the image interaction negligible. For example, increasing the unit cell from 25 × 25 × 15 to 27 × 27 × 15 Å for $*CH_2CH_2OH$ adsorbed on NGQDs leads to a relative energy difference of less than 0.01 eV. The migration paths and barriers during structural transitions were determined by the climbing image nudged elastic band (CI-NEB) method.[49] Similar to the study on Cu substrates, the migration processes were explored in both direct hydrogenation and H-shuttling models.[8] For simplicity, we only considered one water molecule in our simulations. Following the seminal work by Nørskov et al.,[50] computational hydrogen electrode models were employed to obtain thermodynamic free energies of related intermediate products. Free energies are defined as $G = E_{DFT} + E_{ZPE} - TS$, where E_{DFT} and E_{ZPE} are DFT ground state energy and zero-point energy, respectively, on the basis of harmonic approximation taking the vibration frequencies from DFT. Following the same procedure proposed by Peterson et al.,[4] the stabilization energies for adsorbed *COOH and *CO resulting from solvation effects were set to 0.25 and 0.1 eV, respectively. A further −0.33 eV correction for the CO molecule has been derived to accurately describe reaction free energy for CO_2 reduction to CO. These choices predict overpotentials for generating $COOH^-$, CO, and CH_4 reasonably well.

3. RESULTS AND DISCUSSION

In our previous work,[48] we have experimentally discovered that NGQDs with predominant pyridinic N doping at exposed edges are capable of electrocatalytically reducing CO_2 into C_2 hydrocarbons (e.g., C_2H_4) and oxygenate (e.g., C_2H_5OH) in preference to C_1 products (e.g., CO, $HCOO^-$, and CH_4) at relatively low overpotentials (Figure 2). With an applied

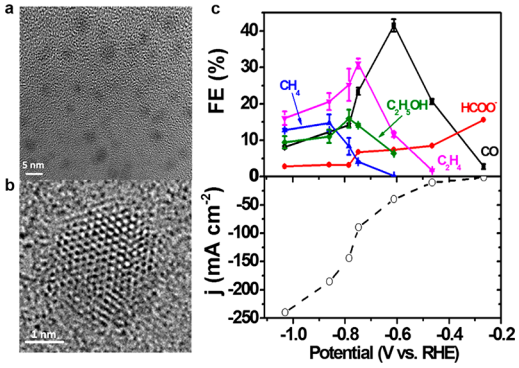

Figure 2. (a) Transmission electron microscopy (TEM) image of NGQDs. (b) High-resolution TEM image of a single NGQD. (c) Dependence of product distribution and total current density of CO_2 reduction over NGQDs on applied potentials. The performance was measured in a flow cell with 1 M KOH as the electrolyte, and the data are compiled from ref 48.

potential more cathodic than −0.6 V, the production of C_2H_4 and C_2H_5OH is predominant with a total maximum Faradaic yield of 45% at −0.75 V. The C_1 hydrocarbon CH_4 is also produced at potentials beyond −0.6 V, but its yield is lower than that of C_2H_4. At lower overpotentials, the primary products are $HCOO^-$ and CO, especially CO, which are formed via a two-electron-transfer pathway.

To begin with theoretical discussions on reaction pathways, we first studied the formation of C_1 hydrocarbon species, which proceed as follows:[4,25] $CO_2 \rightarrow *COOH \rightarrow *CO \rightarrow *COH/*CHO \rightarrow *CHOH/CH_2O \rightarrow *CH_2OH \rightarrow *CH_2/CH_3OH \rightarrow *CH_3 \rightarrow CH_4$. For brevity, the proton–electron couple (H^+ +

DOI: 10.1021/acscatal.7b01839
ACS Catal. 2017, 7, 6245–6250

e^-) and H_2O are omitted. Figure 3a shows the lowest-overpotential pathway for CO_2 reduction to CH_4, while Figure

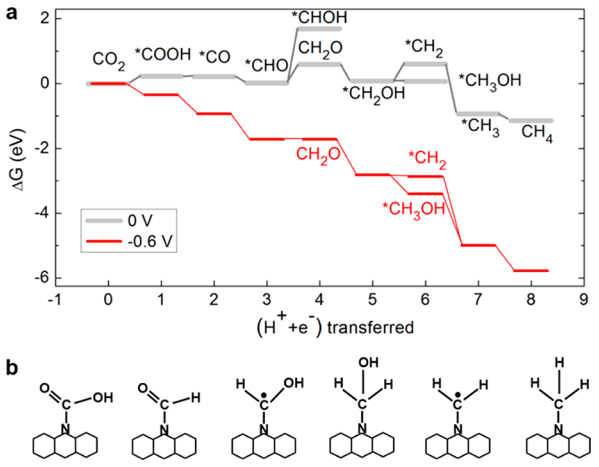

Figure 3. (a) Energy pathways for electrochemical reduction of CO_2 to CH_3OH and CH_4 at 0 V (black) and −0.6 V (red). (b) Schematic for selected intermediate states, including *COOH, *CHO, *CHOH, $*CH_2OH$, $*CH_2$, and $*CH_3$ adsorbed on NGQDs.

3b presents a schematic for various representative intermediate structures. The free energies are given at a potential of 0 V and a theoretical onset potential of −0.6 V vs the standard hydrogen electrode (SHE). In comparison with the results in Figure 2c for the production of CH_4, the calculated onset potential is in good agreement with the experimental value. During the whole 8e transfer process, we mainly focused on three critical steps: (1) the adsorption of *COOH, (2) the formation of *COH or *CHO, and (3) the formation of CH_3OH or $*CH_2$—the precursor of CH_4. The adsorption of *COOH is the rate-limiting step to produce CO. According to the Sabatier principle, the performance of catalysts is determined by the thermodynamic free energy of intermediate states. Figure 4a shows the calculated free energies for *COOH

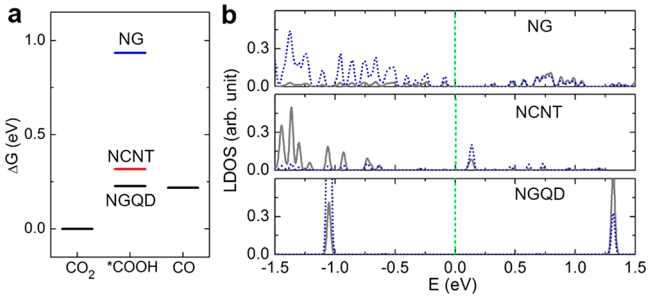

Figure 4. (a) Thermodynamic free energy diagram for the conversion of CO_2 to CO on different N-doped carbon materials, with adsorbed *COOH as the intermediate state. (b) LDOS for pyridinic N (blue dotted lines) and C atoms (gray lines) from adsorbed *COOH. These two atoms form N−C bonds in the intermediate states. Here, NG and NCNT represent N-doped graphene and CNTs, respectively.

on N-doped graphene, CNT, and GQD, respectively. For N-doped graphene, the binding of *COOH is not effective, with its energy being 0.9 eV higher than the initial state (CO_2 + H^+ + e^-). The introduction of curvatures in CNTs or edges in GQDs significantly strengthens the binding of *COOH, and thus the (thermodynamic) barriers for the formation of intermediates are reduced to 0.3 and 0.2 eV in the CNT and GQD cases, respectively. To understand the origin of enhanced binding, we plot the local density of states (LDOS) for intermediate *COOH over all three types of carbon catalysts in Figure 4b. Since the binding between *COOH and substrates is determined by N−C bonds, we only focus on the LDOS for pyridinic N and the C atom from the *COOH group. The first overlapped frontier peak between N and C LDOS appears at 0.1, 0.7, and 1 eV below the Fermi level for N-doped graphene, CNT, and GQD, respectively. The significantly lower position of this peak for N-doped GQD and CNT suggests a much larger energy gain through the formation of N−C bonds in comparison to N-doped graphene.

Following the production of CO, the second key step is the protonation of adsorbed CO to form either adsorbed *COH or *CHO. In the case of Cu, the formation of *COH versus *CHO is critical to determine the selective production of either methane or methanol. The favorable formation of *COH on Cu (by about 0.15 eV) has been suggested to lead to the preferred formation of methane.[8] Following the *COH path, undercoordinated C atoms in intermediate states, such as *COH or even graphitic C, can sit at *hcp* hollow sites of Cu surfaces and favorably bond with several Cu atoms. In the case of NGQD, *COH can only bond to a pyridinic N atom, leaving the C atom undercoordinated, while *CHO can turn into a fully saturated aldehyde structure after the formation of a C−N bond. Therefore, the energy of *COH is 1.9 eV higher than that of *CHO, and the reduction of CO_2 follows the *CHO path to form intermediate formaldehyde (CH_2O). On Cu substrate, the reduction of formaldehyde leads to CH_3OH through intermediate $*OCH_3$. The favorable formation of Cu−O bonds is due to the large difference in electronegativity between Cu and O. In contrast, the formation of $*OCH_3$ is highly unfavorable on NGQDs with an energy 1.56 eV higher than that for $*CH_2OH$ formation through the hydrogenation of O atoms. These results show that the formation of *CHO is the key step for the formation of C_1 hydrocarbon products on NGQDs.

The further hydrogenation of either a C or O atom in $*CH_2OH$ is another major branching point which leads to formation of either CH_3OH or $*CH_2$, respectively. Our thermodynamic analysis shows that the formation of $*CH_2$ through the hydrogenation of O atoms in $*CH_2OH$ is 0.5 eV higher in energy than CH_3OH formation via the hydrogenation of C atoms in $*CH_2OH$, again due to the low coordination of C atoms in $*CH_2$. However, in our electrochemical experiments, only CH_4 was observed during CO_2 reduction on NGQDs. To resolve the discrepancy between thermodynamics and experiments, we proceeded to investigate possible kinetic processes governing the hydrogenation of $*CH_2OH$ to form CH_3OH versus $*CH_2$. Previously, Nie et al.[8] have shown that both the formation of polar O−H bonds and the dissociation of polar C−OH bonds are facilitated by water-assisted proton shuttling coupled with electron transfer, while the formation of relatively more neutral C−H bonds prefers direct hydrogenation from an adsorbed *H. Similarly, if the dissociation of C−OH in $*CH_2OH$ on NGQDs adopts the direct hydrogenation process, a barrier as high as 1.9 eV would emerge. In the transition-state configuration (middle panel in the first row of Figure 5b), two carbon atoms (C atom in the $*CH_2$ group and nearest-neighbor zigzag edge C atom) experience notable distortion. Meanwhile, one O−H bond in the H_2O molecule is stretched to 1.18 Å, representing a 20% increase in comparison

DOI: 10.1021/acscatal.7b01839
ACS Catal. 2017, 7, 6245−6250

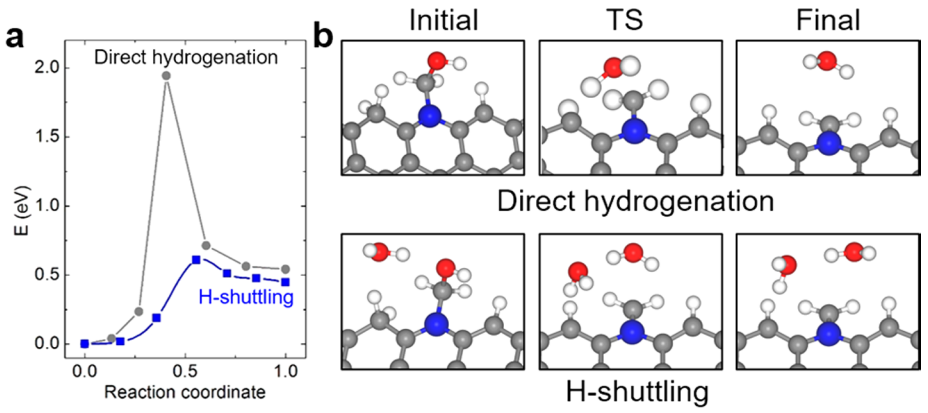

Figure 5. (a) Minimum energy paths for the reduction from *CH_2OH to *CH_2 via either direct hydrogenation (circles) or H-shuttling (squares) mechanisms. (b) Left, middle, and right panels present the initial, transition-state, and final configurations through direct hydrogenation and H-shuttling pathways. Gray, red, large blue, and small white spheres represent carbon, oxygen, nitrogen, and hydrogen atoms, respectively.

to the ground state. All these factors induce the significant energy barrier for C−OH dissociation. The introduction of additional H_2O molecules, which enables H shuttling for the dissociation process, greatly mitigates the distortion of C atoms and O−H bonds, reducing the barrier to only 0.6 eV. On the other hand, the hydrogenation of the C atom in *CH_2OH requires a barrier of 1.7 eV to produce CH_3OH. Assuming the attempting frequencies are similar, the yield of products is mainly determined by the barrier according to transition state theory. The significant difference in barriers renders the selectivity ratio for *CH_2 over CH_3OH on the order of 10^{18}. The further hydrogenation of *CH_2 would produce CH_4 effectively, which is consistent with experimental observations.

Next, we discuss the possible pathways for the production of C_2 species C_2H_4 and C_2H_5OH, with the free energy diagram shown in Figure 6a. The formation of *CH_2 with formal three-coordination makes it highly active to couple with other reactants, including protons, forming the aforementioned CH_4, as well as CO molecules, producing C_2 species. To make the symbolic descriptions for various intermediate structures clearer, we denote these states by *$CH_xO_yCH_{x'}O_{y'}$ where CH_xO_y represents the unit binding to pyridinic N followed by the second $CH_{x'}O_{y'}$ unit, unless otherwise noted. For example, the coupling of *CH_2 and CO forms *CH_2CO with *CH_2 and CO connecting with pyridinic N and the nearest-neighbor zigzag edge C atom (denoted C_Z hereafter) as shown in panel 0 in Figure 6b. The *CH_2CO has both of its C atoms four-coordinated, leading to a notable energy gain of 0.8 eV in comparison to separated *CH_2 and CO. The hydrogenation of C atoms in *CH_2CO could produce either *CH_2CHO or *$COCH_3$ (*$COCH_3$ binds with substrates through the C_Z atom rather than pyridinic N; see panel 1 in Figure 6b). The energy of *CH_2CHO is only 0.25 eV higher than that of *$COCH_3$. Both products can be further hydrogenated, forming acetaldehyde (CH_3CHO) through the proton−electron transfer to C atoms bonding with substrates. On the other hand, the hydrogenation of the O atom in *CH_2CHO leads to *CH_2CHOH, which is about 0.65 eV higher in energy than CH_3CHO.

Similar to the favorable protonation of oxygen over carbon atom in *CH_2OH resulting in CH_4 formation, the barrier is as high as 1.15 eV for direct hydrogenation of the C atom in *$COCH_3$ to form CH_3CHO. In contrast, the barrier decreases to 0.65 eV for hydrogenation of the O atom in *CH_2CHO through H shuttling coupled with electron transfer. Therefore,

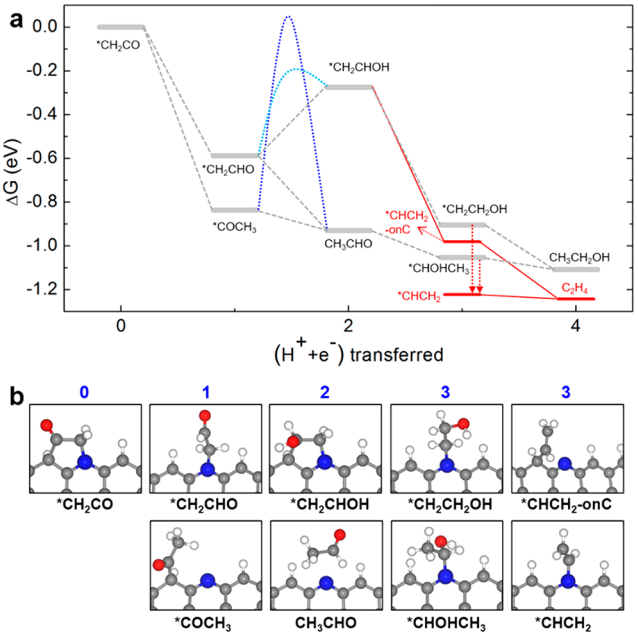

Figure 6. (a) Energy pathways for electrochemical reduction of coupled CH_2 + CO to CH_3CH_2OH and C_2H_4 at 0 V vs SHE. Note that our starting point corresponding to the fact that four $H^+ + e^-$ pairs have been introduced in the Cu case; therefore, only another four steps are required to produce CH_3CH_2OH or C_2H_4. The dotted lines schematically show the barriers for corresponding processes, and the vertical arrows represent the dehydration process. The solid lines highlight the pathways to form C_2H_4. (b) Relaxed configurations for selected intermediate states with different numbers of hydrogen atoms introduced. The numbers at the top indicates how many $H^+ + e^-$ pairs have been transferred in the corresponding panels. Gray, red, large blue, and small white spheres represent carbon, oxygen, nitrogen, and hydrogen atoms, respectively.

even after the higher thermodynamic energy of *CH_2CHO is counted (0.25 eV), the protonation of the O atom is still kinetically favored, forming *CH_2CHOH. Such a comparison is schematically illustrated by the dotted lines in Figure 6a. Through the protonation of C and O atoms, the *CH_2CHOH could be further reduced to either *CH_2CH_2OH or *$CHCH_2$—onC (here, "onC" indicates that *$CHCH_2$ bonds with C_Z rather than pyridinic N)—precursors for C_2H_5OH and C_2H_4, respectively. Given the generally lower barrier for

DOI: 10.1021/acscatal.7b01839
ACS Catal. 2017, 7, 6245−6250

protonation of O over C as discussed above, both thermodynamic and kinetic analyses suggest the higher yield of C_2H_4 by the $*CH_2CHOH$ path. On the other hand, by the CH_3CHO path, the formation of $*CHOHCH_3$ is 0.15 eV lower in energy than that of $*CH_2CH_2OH$. Although $*CHOHCH_3$ can be reduced to C_2H_5OH, its dehydration generates $*CHCH_2$ (the precursor of C_2H_4) with lower energy in comparison to $*CHOHCH_3$ and $*CH_2CH_2OH$ (precursors for C_2H_5OH), again supporting the higher yield of C_2H_4 as observed in our experiment.

It is worth making a comparison between $*CH_2$ + CO coupling on NGQDs and the C−C bond formation through CO dimerization on the Cu surface.[7,9,10] Thermodynamically, the CO dimerization has been shown to be the rate-determining step on the Cu surface with the energy for $*C_2O_2$ being about 0.56 eV higher than the state of two free CO molecules.[7] The dimerization process is facilitated by the abundant active sites of the Cu surface, which adsorb CO with binding energies of 0.25 eV. In the case of NGQD, a similar process would form $*C_2O_2$ in which two C atoms bond with pyridinic N and C_Z atoms, respectively. The energy of $*C_2O_2$ is about 0.58 eV higher than that of two free CO molecules, close to the Cu case. However, NGQDs could not provide enough active sites, given the overall low concentration of edge N dopants. In addition, the CO dimerization process on the Cu substrate is mediated by an electron transfer to form $*C_2O_2^-$, and the transferred electron is mainly located at the O atom, as supported by a Bader charge analysis.[7] The negatively charged O acts as a strong nucleophile and thus becomes easily hydrogenated. In contrast, $*C_2O_2$ on NGQDs is almost neutral, due to the similar electronegativities of adsorbates and substrate. These comparisons suggest a low possibility of the formation of C−C bond through a CO dimerization process on NGQDs.

It should be noted that our calculated barriers are based on the constant-charge condition rather than the constant-voltage condition in electrochemical experiments. To explicitly include the effects of applied potential, Rossmeisl et al.[51] proposed the electrified solid−liquid interface model, in which additional hydrogen atoms are solvated into water. Solid substrates and water layers become charged by protons and electrons, respectively. The internal definition of potential can be obtained from the work function self-consistently. This model has been successfully applied to the hydrogen oxidation/evolution reaction[52] and CRR on Pt(111).[53] Following a similar but simplified approach, the change in barriers versus the applied potential can be obtained qualitatively. We take the hydrogenation reaction of $*CH_2OH$ to $*CH_2$ on NGQDs with five H_2O molecules as an example. When one additional proton is introduced to the nearest H_2O molecule, the structural optimization directly leads to the formation of $*CH_2$ and six H_2O molecules, while the proton can be stabilized at the farthest H_2O molecule. This result indicates that the formation of $*CH_2$ will only need to overcome the barrier of proton transfer from the farthest to the nearest H_2O molecule after the proton is introduced. The barrier of proton transfer in solution is usually on the order of 1−5 kcal/mol (0.04−0.2 eV),[54] much lower than that in the water-solvated proton-free case discussed above (0.6 eV). To show the influences of water-solvated protons on the potential, the positions of highest occupied molecular orbitals (HOMO) for $*CH_2OH$ on NGQDs with and without one additional proton are calculated. The HOMO shifts higher by about 0.6 eV after the introduction of one proton, suggesting that a more negative potential is applied. The more negative potential leads to the decreased barrier, which is consistent with previous results.[52,53] The detailed dependence of the barriers for different hydrogenation processes on applied potential and the influences on the relative yield of diverse products deserve further comprehensive studies.

4. CONCLUSIONS

In summary, adopting DFT simulations, we have studied possible pathways for electrochemical reduction of CO_2 on NGQDs, a metal-free carbon nanostructured catalyst, which demonstrates attractive catalytic activities comparable to those of copper. The N-doped edges bind *COOH significantly more strongly in comparison to N-doped graphene, endowing its higher performance in converting CO_2 to CO. Detailed investigations on both thermodynamics and kinetics show that the kinetics determines the selective generation of CH_4 rather than CH_3OH by forming the key intermediate of $*CH_2$. In the subsequent step, the effective coupling between $*CH_2$ and CO leads to various C_2 products including C_2H_4 and C_2H_5OH, with a higher yield of C_2H_4. These analyses provide a theoretical understanding of the underlying mechanisms for the yield of high-order hydrocarbons and oxygenates, facilitating the design of metal-free catalysts for electrochemical activation and conversion of CO_2.

AUTHOR INFORMATION

Corresponding Authors

*E-mail for X.Z.: xlzou@sz.tsinghua.edu.cn.
*E-mail for B.I.Y.: biy@rice.edu.

ORCID

Xiaolong Zou: 0000-0002-3987-6865
Mingjie Liu: 0000-0002-5341-4448
Jingjie Wu: 0000-0001-6617-0895
Bilu Liu: 0000-0002-7274-5752

Notes

The authors declare no competing financial interest.

ACKNOWLEDGMENTS

This work was supported by the Development and Reform Commission of Shenzhen Municipality under the "Low-Dimensional Materials and Devices Discipline", the Youth 1000-Talent Program of China, and the Tsinghua-Berkeley Shenzhen Institute (TBSI). X.Z., M.L., and B.I.Y. acknowledge support by the Robert Welch Foundation (C-1590).

REFERENCES

(1) Kuhl, K. P.; Cave, E. R.; Abram, D. N.; Jaramillo, T. F. *Energy Environ. Sci.* **2012**, *5*, 7050−7059.
(2) Hori, Y.; Wakebe, H.; Tsukamoto, T.; Koga, O. *Electrochim. Acta* **1994**, *39*, 1833−1839.
(3) Hori, Y.; Murata, A.; Takahashi, R. *J. Chem. Soc., Faraday Trans. 1* **1989**, *85*, 2309−2326.
(4) Peterson, A. A.; Abild-Pedersen, F.; Studt, F.; Rossmeisl, J.; Norskov, J. K. *Energy Environ. Sci.* **2010**, *3*, 1311−1315.
(5) Schouten, K. J. P.; Kwon, Y.; van der Ham, C. J. M.; Qin, Z.; Koper, M. T. M. *Chem. Sci.* **2011**, *2*, 1902−1909.
(6) Hatsukade, T.; Kuhl, K. P.; Cave, E. R.; Abram, D. N.; Jaramillo, T. F. *Phys. Chem. Chem. Phys.* **2014**, *16*, 13814−13819.
(7) Calle-Vallejo, F.; Koper, M. T. M. *Angew. Chem., Int. Ed.* **2013**, *52*, 7282−7285.

DOI: 10.1021/acscatal.7b01839
ACS Catal. 2017, 7, 6245−6250

(8) Nie, X. W.; Esopi, M. R.; Janik, M. J.; Asthagiri, A. *Angew. Chem., Int. Ed.* **2013**, *52*, 2459−2462.
(9) Montoya, J. H.; Peterson, A. A.; Norskov, J. K. *ChemCatChem* **2013**, *5*, 737−742.
(10) Montoya, J. H.; Shi, C.; Chan, K.; Norskov, J. K. *J. Phys. Chem. Lett.* **2015**, *6*, 2032−2037.
(11) Sen, S.; Liu, D.; Palmore, G. T. R. *ACS Catal.* **2014**, *4*, 3091−3095.
(12) Xiao, H.; Cheng, T.; Goddard, W. A.; Sundararaman, R. *J. Am. Chem. Soc.* **2016**, *138*, 483−486.
(13) Goodpaster, J. D.; Bell, A. T.; Head-Gordon, M. *J. Phys. Chem. Lett.* **2016**, *7*, 1471−1477.
(14) Schouten, K. J. P.; Qin, Z. S.; Gallent, E. P.; Koper, M. T. M. *J. Am. Chem. Soc.* **2012**, *134*, 9864−9867.
(15) Zhu, D. D.; Liu, J. L.; Qiao, S. Z. *Adv. Mater.* **2016**, *28*, 3423−3452.
(16) Li, Y. W.; Sun, Q. *Adv. Energy Mater.* **2016**, *6*, 1600463.
(17) Luo, W. J.; Nie, X. W.; Janik, M. J.; Asthagiri, A. *ACS Catal.* **2016**, *6*, 219−229.
(18) Verdaguer-Casadevall, A.; Li, C. W.; Johansson, T. P.; Scott, S. B.; McKeown, J. T.; Kumar, M.; Stephens, I. E. L.; Kanan, M. W.; Chorkendorff, I. *J. Am. Chem. Soc.* **2015**, *137*, 9808−9811.
(19) Li, C. W.; Ciston, J.; Kanan, M. W. *Nature* **2014**, *508*, 504−507.
(20) Ma, S.; Sadakiyo, M.; Heima, M.; Luo, R.; Haasch, R. T.; Gold, J. I.; Yamauchi, M.; Kenis, P. J. A. *J. Am. Chem. Soc.* **2017**, *139*, 47−50.
(21) Mistry, H.; Varela, A. S.; Bonifacio, C. S.; Zegkinoglou, I.; Sinev, I.; Choi, Y. W.; Kisslinger, K.; Stach, E. A.; Yang, J. C.; Strasser, P.; Cuenya, B. R. *Nat. Commun.* **2016**, *7*, 12123.
(22) Kas, R.; Hummadi, K. K.; Kortlever, R.; de Wit, P.; Milbrat, A.; Luiten-Olieman, M. W. J.; Benes, N. E.; Koper, M. T. M.; Mul, G. *Nat. Commun.* **2016**, *7*, 10748.
(23) Zhao, Z. L.; Chen, Z. Z.; Zhang, X.; Lu, G. *J. Phys. Chem. C* **2016**, *120*, 28125−28130.
(24) Ma, X. F.; Li, Z.; Achenie, L. E. K.; Xin, H. L. *J. Phys. Chem. Lett.* **2015**, *6*, 3528−3533.
(25) Kortlever, R.; Shen, J.; Schouten, K. J. P.; Calle-Vallejo, F.; Koper, M. T. M. *J. Phys. Chem. Lett.* **2015**, *6*, 4073−4082.
(26) Hong, X.; Chan, K. R.; Tsai, C.; Norskov, J. K. *ACS Catal.* **2016**, *6*, 4428−4437.
(27) Shen, H. M.; Li, Y. W.; Sun, Q. *J. Phys. Chem. C* **2017**, *121*, 3963−3969.
(28) Yang, L. J.; Jiang, S. J.; Zhao, Y.; Zhu, L.; Chen, S.; Wang, X. Z.; Wu, Q.; Ma, J.; Ma, Y. W.; Hu, Z. *Angew. Chem., Int. Ed.* **2011**, *50*, 7132−7135.
(29) Liang, J.; Jiao, Y.; Jaroniec, M.; Qiao, S. Z. *Angew. Chem., Int. Ed.* **2012**, *51*, 11496−11500.
(30) Gong, K. P.; Du, F.; Xia, Z. H.; Durstock, M.; Dai, L. M. *Science* **2009**, *323*, 760−764.
(31) Yang, S. B.; Feng, X. L.; Wang, X. C.; Mullen, K. *Angew. Chem., Int. Ed.* **2011**, *50*, 5339−5343.
(32) Qu, L. T.; Liu, Y.; Baek, J. B.; Dai, L. M. *ACS Nano* **2010**, *4*, 1321−1326.
(33) Tang, Y. F.; Allen, B. L.; Kauffman, D. R.; Star, A. *J. Am. Chem. Soc.* **2009**, *131*, 13200−13201.
(34) Kumar, B.; Asadi, M.; Pisasale, D.; Sinha-Ray, S.; Rosen, B. A.; Haasch, R.; Abiade, J.; Yarin, A. L.; Salehi-Khojin, A. *Nat. Commun.* **2013**, *4*, 2819.
(35) Wu, J. J.; Yadav, R. M.; Liu, M. J.; Sharma, P. P.; Tiwary, C. S.; Ma, L. L.; Zou, X. L.; Zhou, X. D.; Yakobson, B. I.; Lou, J.; Ajayan, P. M. *ACS Nano* **2015**, *9*, 5364−5371.
(36) Zhang, S.; Kang, P.; Ubnoske, S.; Brennaman, M. K.; Song, N.; House, R. L.; Glass, J. T.; Meyer, T. J. *J. Am. Chem. Soc.* **2014**, *136*, 7845−7848.
(37) Wu, J. J.; Liu, M. J.; Sharma, P. P.; Yadav, R. M.; Ma, L. L.; Yang, Y. C.; Zou, X. L.; Zhou, X. D.; Vajtai, R.; Yakobson, B. I.; Lou, J.; Ajayan, P. M. *Nano Lett.* **2016**, *16*, 466−470.
(38) Zhu, G. Z.; Li, Y. W.; Zhu, H. Y.; Su, H. B.; Chan, S. H.; Sun, Q. *Nano Res.* **2017**, *10*, 1641−1650.
(39) Li, Q. Q.; Zhang, S.; Dai, L. M.; Li, L. S. *J. Am. Chem. Soc.* **2012**, *134*, 18932−18935.
(40) Favaro, M.; Ferrighi, L.; Fazio, G.; Colazzo, L.; Di Vaentin, C.; Durante, C.; Sedona, F.; Gennaro, A.; Agnoli, S.; Granozzi, G. *ACS Catal.* **2015**, *5*, 129−144.
(41) Gong, Y. J.; Fei, H. L.; Zou, X. L.; Zhou, W.; Yang, S. B.; Ye, G. L.; Liu, Z.; Peng, Z. W.; Lou, J.; Vajtai, R.; Yakobson, B. I.; Tour, J. M.; Ajayan, P. M. *Chem. Mater.* **2015**, *27*, 1181−1186.
(42) Kresse, G.; Furthmuller, J. *Comput. Mater. Sci.* **1996**, *6*, 15−50.
(43) Kresse, G.; Furthmuller, J. *Phys. Rev. B: Condens. Matter Mater. Phys.* **1996**, *54*, 11169−11186.
(44) Perdew, J. P.; Burke, K.; Ernzerhof, M. *Phys. Rev. Lett.* **1996**, *77*, 3865−3868.
(45) Blochl, P. E. *Phys. Rev. B: Condens. Matter Mater. Phys.* **1994**, *50*, 17953−17979.
(46) Kresse, G.; Joubert, D. *Phys. Rev. B: Condens. Matter Mater. Phys.* **1999**, *59*, 1758−1775.
(47) Guo, D. H.; Shibuya, R.; Akiba, C.; Saji, S.; Kondo, T.; Nakamura, J. *Science* **2016**, *351*, 361−365.
(48) Wu, J. J.; Ma, S. C.; Sun, J.; Gold, J. I.; Tiwary, C.; Kim, B.; Zhu, L. Y.; Chopra, N.; Odeh, I. N.; Vajtai, R.; Yu, A. Z.; Luo, R.; Lou, J.; Ding, G. Q.; Kenis, P. J. A.; Ajayan, P. M. *Nat. Commun.* **2016**, *7*, 13869.
(49) Henkelman, G.; Uberuaga, B. P.; Jonsson, H. *J. Chem. Phys.* **2000**, *113*, 9901−9904.
(50) Norskov, J. K.; Rossmeisl, J.; Logadottir, A.; Lindqvist, L.; Kitchin, J. R.; Bligaard, T.; Jonsson, H. *J. Phys. Chem. B* **2004**, *108*, 17886−17892.
(51) Rossmeisl, J.; Skulason, E.; Bjorketun, M. E.; Tripkovic, V.; Norskov, J. K. *Chem. Phys. Lett.* **2008**, *466*, 68−71.
(52) Skulason, E.; Tripkovic, V.; Bjorketun, M. E.; Gudmundsdottir, S.; Karlberg, G.; Rossmeisl, J.; Bligaard, T.; Jonsson, H.; Norskov, J. K. *J. Phys. Chem. C* **2010**, *114*, 18182−18197.
(53) Hussain, J.; Jonsson, H.; Skulason, E. *Faraday Discuss.* **2016**, *195*, 619−636.
(54) Guthrie, J. P. *J. Am. Chem. Soc.* **1996**, *118*, 12886−12890.

DOI: 10.1021/acscatal.7b01839
ACS Catal. 2017, 7, 6245−6250